Compensation for multimode fiber dispersion by adaptive optics

Xiling Shen, Joseph M. Kahn, and Mark A. Horowitz

Department of Electrical Engineering, Stanford University, Stanford, California 94305

Received May 25, 2005; revised manuscript received July 20, 2005; accepted July 21, 2005

Adaptive optics is used to compensate for modal dispersion in digital transmission through multimode fiber (MMF). At the transmitter, a spatial light modulator (SLM) controls the launched field pattern. An estimate of intersymbol interference (ISI) caused by modal dispersion is formed at the receiver and fed back to the transmitter, where the SLM is adjusted to minimize ISI. Error-free transmission of 10 Gbit/s non-return-to-zero signals through standard 50 μm graded-index MMFs up to 11.1 km long is demonstrated. It is shown that a single SLM can compensate for modal dispersion across a 600 GHz bandwidth. © 2005 Optical Society of America

OCIS codes: 010.1080, 060.2330, 060.2360, 060.4510, 070.2580, 070.6020.

Multimode fiber (MMF) is widely employed in local- and campus-area networks. It would be useful to transmit data at 10 Gbits/s and higher bit rates over multikilometer lengths of MMF, but modal dispersion limits transmission length at these high bit rates. Various approaches have been taken to increase the bit-rate–length product in existing[1,2] or MMFs. Principal modes (PMs) in MMF propagate independently and with well-defined group delays (to first order in frequency), even in the presence of modal coupling.[4] PMs are the generalization to MMF of the principal states of polarization found in single-mode fiber (SMF) with polarization dispersion.[5] Like principal states of polarization in SMF, PMs in MMF evolve as the fiber changes in response to time-varying perturbations, e.g., temperature and vibration. It is demonstrated here that adaptive optics can effectively learn and track the time-varying PMs in MMF, thus compensating for modal dispersion.[6]

The experimental system is shown in Fig. 1. A *C*-band laser can be tuned to a comb of 100 channels, spaced by 50 GHz, over the 1527–1567 nm wavelength range. A Mach–Zehnder modulator encodes a chirp-free 10 Gbit/s non-return-to-zero signal that has +6 dBm average power, which is output into a polarization-maintaining SMF (PM-SMF) that has a numerical aperture (NA) of 0.11. The PM-SMF output, in the LP_{01} mode, is collimated by an $f = 10.4$ mm plano–convex lens and illuminates a spatial light modulator (SLM); a half-wave ($\lambda/2$) plate aligns the PM-SMF output to the linear state of polarization (SOP) required at the SLM. The nematic liquid-crystal phase-only SLM has 256×256 pixels, each 18 μm $\times$ 18 μm in size, each independently controllable with 5–6 bit resolution over the range $0-2\pi$, with switching times of $\leqslant 50$ ms ($\pi \leftrightarrow 2\pi, 10\% \leftrightarrow 90\%$).

After reflecting from the SLM and passing through a 45%–45% polarization-independent beam splitter, the beam is coupled into a MMF through an $f = 10.4$ mm plano–convex lens, resulting in a launched NA of 0.11. The beam spot is nominally center launched to excite lower-order modes (LOMs) preferentially. A half-wave plate and a quarter-wave ($\lambda/4$) plate allow the launched signal to be adjusted to an arbitrary SOP. The free-space optical system has a loss of ~ -8.5 dB, so an average power of ~ -2.5 dBm is launched (for a blank SLM pattern). Test fibers are spooled, plastic-jacketed, standard 50 μm graded-index MMFs that have power-law index profiles with exponents of 2.00–2.03 and a NA of 0.19 at *C*-band wavelengths. For test fibers of lengths 1030, 3100, and 11081 m, the received optical power

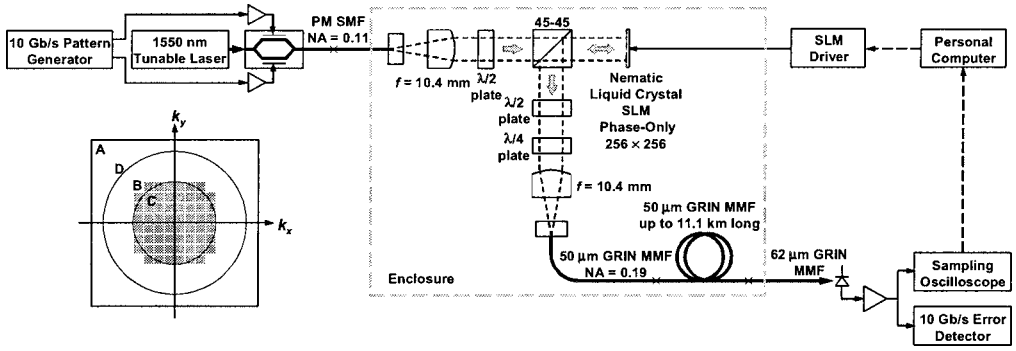

Fig. 1. Experimental setup. Inset, SLM in the Fourier plane of the input face of a MMF. A, Boundary of the SLM active region; B, block structure of the SLM pattern; C, circle enclosing 95% of the power of the beam incident onto the SLM, corresponding to a NA of 0.11 at the MMF input; D, circle corresponding to the MMF's NA of 0.19. GRIN, gradient index; Gb/s, Gbit/s.

0146-9592/05/222985-3/$15.00

is approximately −3.4, −3.9, and −5.5 dBm, respectively (for a blank SLM pattern).

The test fiber output is connected via a 62.5 μm MMF pigtail to a commercial receiver that comprises an InGaAs p-i-n photodiode and transimpedance preamplifier and has a dc −9.5 GHz bandwidth (at −3 dB). The sensitivity and the overload power are −20 and +2 dBm, respectively, both at a 10^{-10} bit-error ratio. When intersymbol interference (ISI) is reduced sufficiently, error-free reception is observed (defined here as 0 errors in 10^{11} bits). Receiver electrical output waveforms are acquired by a sampling oscilloscope and sent via a general-purpose interface bus (GPIB) to a personal computer, which estimates ISI, executes an adaptive algorithm, and controls the SLM.

The SLM, situated in the Fourier plane of the MMF input, performs spatial signal processing. The SLM surface is depicted in the inset of Fig. 1. Coordinates on the SLM are denoted by spatial frequencies k_x and k_y, where A denotes the boundary of the 256×256 pixel active region. To reduce complexity, 16×16 blocks of pixels are grouped together and are restricted to take on binary phase values in the set $\{\pi,2\pi\}$. A set of 60 such blocks, denoted B, is used. This set covers a circle enclosing 95% of the energy of the incident LP_{01} mode of the PM-SMF, denoted C, which corresponds to a NA of 0.11 in the MMF. Circle D denotes a MMF NA of 0.19. Restricting launched spatial frequencies to a NA of 0.11 reduces excitation of higher-order modes (HOMs) at launch; whereas it may also diminish the SLM's control over HOMs that are coupled into during propagation, this trade-off has been found empirically to yield good results.

By controlling the launched field pattern, the SLM controls the MMF impulse response. Neglecting group-velocity dispersion, the MMF input and output intensity waveforms are related by linear convolution $I_{\mathrm{out}}(t)=I_{\mathrm{in}}(t)*h(t)$, where $h(t)$ is the MMF impulse response. Observe that $h(t)\geqslant0$, $-\infty<t<\infty$. It can be shown that[4]

$$h(t)\approx\frac{\exp(-\alpha L)}{P_0}\sum_{n=1}^{2N}\left[\mathrm{Re}\int_{\mathrm{SLM}}V(k_x,k_y)\mathbf{E}_0(k_x,k_y)\times\mathbf{H}^{*}_{\mathrm{in},n}(k_x,k_y)\cdot\hat{z}\,\mathrm{d}k_x\mathrm{d}k_y\right]^2\delta(t-\tau_n),\qquad(1)$$

where α is the fiber loss coefficient (approximated as mode independent), L is the fiber length, P_0 is the total incident power, $2N$ is the number of propagating PMs (in all polarizations), $V(k_x,k_y)$ is the SLM reflectance, $\mathbf{E}_0(k_x,k_y)$ is the spatial Fourier transform of the LP_{01} mode electric field incident upon the SLM, $\mathbf{H}_{\mathrm{in},n}(k_x,k_y)$ is the spatial Fourier transform of the nth input PM magnetic field, $\hat{z}$ is a unit vector along the fiber axis, and τ_n is the group delay of the nth PM. Equation (1) shows that $h(t)$ is a sum of impulses from each of the $2N$ PMs, and the weighting of these impulses can be manipulated by changing $V(k_x,k_y)$.

Suppose that an isolated 1 bit is transmitted, described by input intensity waveform $p(t)$, and the receiver impulse response is $r(t)$. The receiver output waveform is given by $g(t)=p(t)*h(t)*r(t)$, which is referred to as the continuous-time system's impulse response. When a sequence of 0 and 1 bits is transmitted and the receiver output is sampled once per bit interval, the effect of ISI is characterized by the discrete-time system's impulse response[7] $g(nT;t_0)=g(t)|_{t_0+nT}$, where n is an integer, T is the bit duration, and t_0 is an initial offset. An objective function that quantifies ISI is[7]

$$F[g(nT;t_0)]=g(0T;t_0)-\sum_{n\neq0}g(nT;t_0)=2g(0T;t_0)-\sum_{n}g(nT;t_0).\qquad(2)$$

At a high signal-to-noise ratio, the effect of ISI on the bit-error ratio depends on $g(nT;t_0)$ only through $F[g(nT;t_0)]$,[7] where $F[g(nT;t_0)]<0$ when the eye is closed and $F[g(nT;t_0)]>0$ when the eye is open. The adaptive algorithm adjusts $V(k_x,k_y)$ to control $h(t)$ [and thus $g(t)$] in an attempt to maximize $F[g(nT;t_0)]$, and it also chooses t_0 to maximize $F[g(nT;t_0)]$.

Each time $V(k_x,k_y)$ is changed, the received waveform is acquired by the sampling oscilloscope for estimation of $F[g(nT;t_0)]$. Eight samples per bit interval are taken to produce sufficient resolution in choosing t_0, and four acquisitions of the waveform are averaged to reduce thermal and quantization noises. When the eye is closed, a periodic training sequence, comprising 64 0 bits followed by 64 1 bits, is transmitted. To estimate $F[g(nT;t_0)]$ we use the largest positive and negative excursions of the received waveform over any intervals of duration T (separated by $64T$) to estimate $\pm g(0T;t_0)$; the total excursion of the received waveform is used to estimate $\Sigma_n g(nT;t_0)$. When the eye is open, a 2^7-1 pseudorandom bit sequence (PRBS) is transmitted, and the eye opening itself is used as an estimate of $F[g(nT;t_0)]$. A single estimation of $F[g(nT;t_0)]$ requires $\sim$0.9 s, which is dominated by waveform sampling and GPIB interface latency.

In a single iteration of the adaptive algorithm, the 60 SLM blocks are flipped ($\pi\rightarrow2\pi$ or $2\pi\rightarrow\pi$) one by one, proceeding outward from the center in concentric rings. If a flip increases the estimate of $F[g(nT;t_0)]$ it is kept; otherwise, it is discarded. Each iteration of 60 flips requires $\sim$55 s. If the eye is initially closed, the first iteration uses the periodic training sequence; otherwise, it uses the 2^7-1 PRBS. All subsequent iterations use the 2^7-1 PRBS.

Figure 2 describes transmission experiments in a 1030 m MMF. Figures 2(a) and 2(b) depict a near-best-case launched SOP; Figs. 2(c) and 2(d) depict a near-worst-case launched SOP, as indicated on Poincaré spheres. For each SOP the two rows depict the SLM pattern, system's impulse response, and eye pattern (for 2^7-1 PRBS) before and after adaptation. Changing the SOP from Figs. 2(a) and 2(b) to Figs. 2(c) and 2(d) increases coupling from LOMs to

HOMs, as is evident in the system's impulse responses $g(t)$. HOMs have longer group delays, consistent with the MMF index profiles. The adaptive algorithm converges whether the initial value of $F[g(nT;t_0)]$ is positive [Fig. 2(a)] or negative [Fig. 2(c)]. Depending on the severity of ISI before adaptation, one to three iterations are required for approaching the largest achievable value of $F[g(nT;t_0)]$. SLM adaptation attenuates HOMs, as is evident in the system impulse responses $g(t)$. Adapted SLM patterns include blocks of π relative phase shifts at higher spatial frequencies, consistent with attenuation of HOMs. SLM adaptation reduces the total launched optical power, which is evident in the areas under the system impulse responses $g(t)$. For every SOP tested, after adaptation error-free reception is achieved for PRBS lengths up to $2^{31}-1$.

Similar experiments have been performed for MMFs of 3100 and 11,081 m length. For every launched SOP tested, whether it resulted in a closed or a partially open eye, the adaptive algorithm converges and yields an open eye pattern. For good and intermediate SOPs, error-free reception is achieved for PRBS lengths up to $2^{31}-1$. For near-worst-case SOPs, error-free reception is achieved only for PRBS lengths up to $2^{10}-1$. These effects are under investigation.

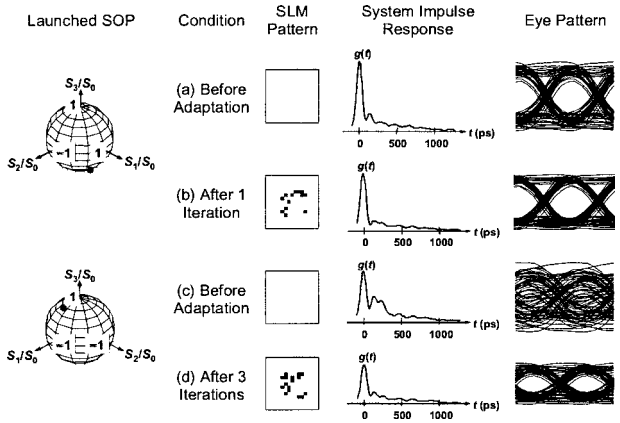

Fig. 2. 10 Gbit/s × 1030 m transmission, demonstrating the effect of a launched SOP.

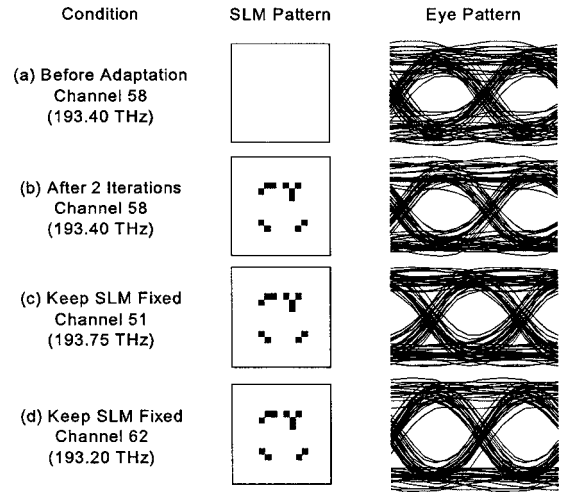

Fig. 3. 10 Gbit/s × 11,081 m transmission in a good launched SOP, demonstrating that one SLM can compensate for modal dispersion across a 600 GHz bandwidth.

Figure 3 illustrates the potential applicability of the scheme to wavelength-division-multiplexed systems. The MMF is 11,081 m long. With the transmitter laser tuned to channel 58 (193.40 THz), before adaptation the half- and quarter-wave plates are adjusted to yield a good launched SOP, resulting in the eye pattern shown in Fig. 3(a). Two iterations of the adaptive algorithm are run, resulting in the SLM pattern and eye pattern shown in Fig. 3(b). Holding the SOP and SLM pattern fixed, we tune the laser to channel 51 (193.75 THz) and to channel 62 (193.20 THz), obtaining the eye patterns shown in Figs. 3(c) and 3(d), respectively. Using the same SOP and SLM pattern for all twelve channels 51,...,62, spanning a 600 GHz bandwidth, we achieved error-free reception for PRBS lengths up to $2^{31}-1$.

The good performance in the longer fibers (3100 and 11,081 m) is perhaps surprising. It appears that differential loss $\Delta\alpha$ between HOMs and LOMs is amplified by long fiber length L, since the received power ratio is $\exp(-\Delta\alpha L)$, reducing $\Sigma_{n\neq 0} g(nT;t_0)$ relative to $g(0T;t_0)$.

The optical compensation scheme offers scalability advantages over electrical compensation schemes. One SLM can serve several wavelength-division multiplexed channels, unlike electrical compensators, which are implemented separately for each channel. The optical technique may scale more easily to high bit rates and long fibers, because requirements on the SLM appear to be substantially independent of bit rate and fiber length. By contrast, for electrical compensators, the number of taps in a finite-impulse-response equalizer is proportional to the bit rate × length product, while the number of states in a maximum-likelihood sequence detector is exponential in that product.

This research was supported by an IBM Faculty Award. The authors are grateful for discussions with S. Fan and with Teresa Ewing and Anna Linnenberger of Boulder Nonlinear Systems. J. M. Kahn's e-mail address is jmk@ee.stanford.edu.

References

1. L. Raddatz, I. H. White, D. G. Cunningham, and M. C. Nowell, IEEE Photonics Technol. Lett. **10**, 534 (1998).
2. K. M. Patel and S. E. Ralph, IEEE Photonics Technol. Lett. **14**, 393 (2002).
3. T. Itoh, H. Fukuyama, S. Tsunashima, E. Yoshida, Y. Yamabayashi, M. Muraguchi, H. Toba, and H. Sugahara, in *Optical Fiber Communication Conference OFC* (Optical Society of America, 2005), paper OWH3.
4. S. Fan and J. M. Kahn, Opt. Lett. **30**, 135 (2005).
5. C. D. Poole and R. E. Wagner, Electron. Lett. **22**, 1029 (1986).
6. E. Alon, V. Stojanović, J. M. Kahn, S. P. Boyd, and M. A. Horowitz, in *Proceedings of the IEEE Global Telecommunications Conference* (Institute of Electrical and Electronics Engineers, 2004), p. 1023.
7. J. M. Kahn, W. J. Krause, and J. B. Carruthers, IEEE Trans. Commun. **43**, 1613 (1995).